DOI: 10.21062/mft.2023.060  http://www.journalmt.com

# Research on Viewpoint Planning Method for Multi-view Image 3D Reconstruction

Yun Shi (0009-0008-4699-7703), Yanyan Zhu (0000-0003-3360-1104)
West Anhui University, Luan, China. E-mail: zhou.dp126@gmail.com

**A model-based viewpoint planning and filtering method is proposed to determine the position and pose of viewpoints in 3D reconstruction of multi-view images. The method first determines the necessary parameters to control the camera position and attitude. Second, the mathematical error model is developed and combined with stereo overlap to guide viewpoint selection. According to the shooting distance, a dense candidate view area is then established, the subview collection is screened, & a view supplement scheme is proposed for the area where the candidate view cannot be shot, improving the integrity of the resulting data. Experimental results demonstrate that our viewpoint planning method has high shooting coverage & highly accurate 3D reconstruction.**

**Keywords:** Multi-view, 3D reconstruction, Aerial-photography, View Planning

## 1 Introduction

Three-dimensional (3D) reconstruction consists of restoring the 3D structure of a measured object using multiple images taken from various angles. It is widely used in various fields including target tracking, reverse engineering, virtual reality, and robot vision [1-15]. Camera viewpoint planning is uncertain and a know how in target reconstruction. Scott and Roth [16] summarized the research on camera viewpoint planning in the field of laser 3D measurement and machine vision. Qiana et al. [13] studied path planning, motion prediction, and collision avoidance for automatic driving technology. The path planning algorithm for autonomous underwater vehicles (AUV) was studied in [20]. The multicellular genetic method was used in [21] to lay out and optimize camera viewpoints. Dunn and Olague [23] established the cost function of viewpoints, and their proposed planning method can reduce the redundancy of shooting viewpoints and improve the accuracy of 3D reconstruction. Schmid and Hirschmuller [24] arranged and screened viewpoints based on the overlap constraint, coverage constraint, and the incident angle constraint of adjacent viewpoints. They arranged the viewpoints according to the rough 3D model of the tested object. Zhen [25,18] studied the extraction of key frames in aerial images and 3D reconstruction for outdoor scenes. Gospodnetić et al. [26, 17] summarized the available generation and test methods and evaluated the results of various objects.

In some special cases involving 3D reconstruction, like target measurement in large outdoor scenes, it can be challenging to gather all the necessary data due to the limited measurement flexibility. When the unmanned aerial vehicle (UAV) is manually operated for shooting, there are issues like repeated and missed shooting, as well as inappropriate shooting angle, which has a significant impact on the integrity and accuracy of the reconstructed data. The navigation path of the UAV is planned using two-dimensional map information. The camera shooting angle is not controlled and adjusted during the navigation process, which makes the subsequent 3D reconstruction difficult. The UAV aerial photography process must therefore be planned, especially the camera shooting viewpoint. UAV aerial photography viewpoint planning needs to use airborne positioning to determine the UAV space position. Due to the low accuracy of airborne positioning, the impact of errors must be considered in planning. This paper proposes a new viewpoint planning method based on the known model. First, the viewpoint candidate areas are arranged, and then the optimal sub-viewpoint set is selected according to the constraints of overlap, incidence angle and shooting coverage under the consideration of error. It is implemented on the independently developed aerial photography UAV and camera position and attitude control platform. [19,22,24]

## 2 Materials and Methods

### 2.1 Network camera pose control parameters

Fig. 1 shows the position and attitude relationship of the earth, the UAV and the camera, where $W_e X_e Y_e Z_e$ represent the geographical coordinate system, $W_u X_u Y_u Z_u$ represent the UAV fuselage coordinate system, $W_c X_c Y_c Z_c$ represent the camera coordinate system, $\boldsymbol{P}_u^e = \left[ x_u^e \ y_u^e \ z_u^e \ \varphi_u^e \ \theta_u^e \ \gamma_u^e \right]^T$ represents the position and attitude of the UAV in the

geographic coordinate system, and $\boldsymbol{P}_c^u = \left[ x_c^u \ y_c^u \ z_c^u \ \varphi_c^u \ \theta_c^u \ \gamma_c^u \right]^T$ is the position and attitude of the camera in the UAV coordinate system.

Multi-rotor UAV realizes flight control by setting $\boldsymbol{P}_u^e$. When the pitch angle $\theta_u^e$ and roll angle $\gamma_u^e$ are not zero, the fuselage will move longitudinally and laterally, respectively. Therefore, when the UAV hovers to take images, it is necessary to ensure $\theta_u^e = \gamma_u^e = 0$. The PTZ fixed under the fuselage provides the changes of the camera's pitch angle $\theta_c^u$ & roll angle $\gamma_c^u$. When $X_c^u = Y_c^u = Z_c^u = \varphi_c^u = 0$, the viewpoint position and attitude of the UAV during aerial photography can be expressed as:

$$\boldsymbol{V} = [x_u^e \quad y_u^e \quad z_u^e \quad \varphi_u^e \quad \theta_c^u \quad \gamma_c^u]^T = [x_v \quad y_v \quad z_v \quad \alpha_v \quad \beta_v \quad \gamma_v]^T \tag{1}$$

Where $x_v$, $y_v$, $z_v$ represent three position degrees of freedom and $\alpha_v$, $\beta_v$, $\gamma_v$ represent three rotation angles.

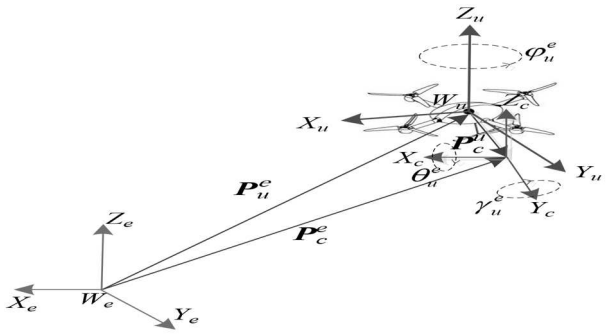


***Fig. 1*** *Position and attitude relationship of the earth, the UAV, and the camera*

## 2.2 Viewpoint constraint

The requirements for 3D reconstruction are visibility constraints, overlap, motion platform constraints, and camera incidence angle.

## 2.3 Visibility constraints

Visibility constraints include visual angle, occlusion, and field of view constraints.

### 2.3.1 Visual angle

Fig. 2 shows a schematic diagram of viewable constraint and occlusion, where *O* is the center of the lens, *P* is the space point, *v* is the shooting direction of the lens, *n* is the normal vector at point *P*, and $\theta$ is the angle between *n* and *v*. When $\theta < 90^o$, the point *P* can be captured by the camera.

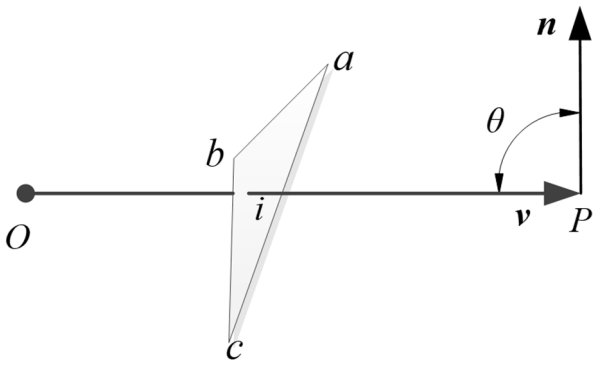


***Fig. 2*** *Diagram of viewable constraint and occlusion*

### 2.3.2 Occlusion

As shown in Fig. 2, the $\Delta abc$ is a patch on the model. The intersection between the triangle patch's plane and the line *OP* is *i*. If the optical path between the lens center and the spatial point *P* is not blocked by the model itself, the condition in (2) must be met:

$$S_{\Delta aib} + S_{\Delta bic} + S_{\Delta cia} > S_{\Delta abc} \tag{2}$$

### 2.3.3 Constraints of the field of vision

As shown in Figure 3, the projection of point *P* on the camera through the small hole is $P'$, and the field of view constraint requires that the line *OP* be within the range of the longitudinal field angle $\alpha$ and the transverse $\beta$, which needs to meet the conditions in (3):

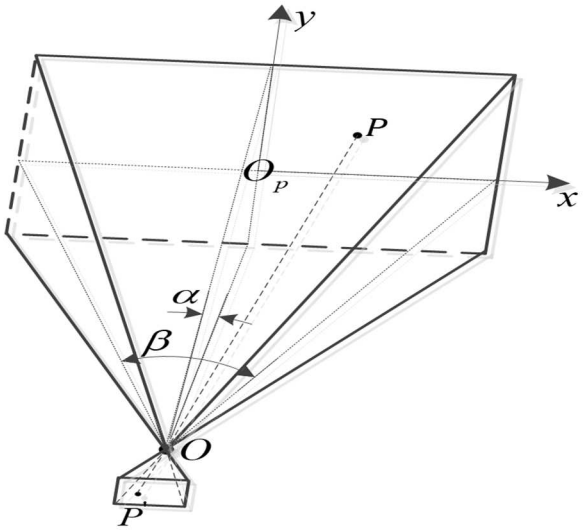


***Fig. 3*** *Schematic diagram of field constraint*

$$\left.\begin{aligned} \boldsymbol{v} \cdot \boldsymbol{v}_{py} - \left\| \boldsymbol{v}_{py} \right\| \cdot \left\| \boldsymbol{v} \right\| \cos(\alpha/2) \geq 0 \\ \boldsymbol{v} \cdot \boldsymbol{v}_{px} - \left\| \boldsymbol{v}_{px} \right\| \cdot \left\| \boldsymbol{v} \right\| \cos(\beta/2) \geq 0 \end{aligned}\right\} \tag{3}$$

Where $\alpha = 61.9^o$, $\beta = 77.32^o$, $\boldsymbol{v}_p$ represents the vector of $\boldsymbol{OP}$, while $\boldsymbol{v}_{px}$ and $\boldsymbol{v}_{py}$ represent the projection loss of $\boldsymbol{v}_p$ on the camera's transverse midplane $xO_pO$, & longitudinal midplane $yO_pO$ respectively.

### 2.4 Overlap and motion platform constraints

Multi-view 3D reconstruction must ensure the degree of overlap between multi-views, which is used for image feature point matching and polar constraint to solve 3D coordinates. In fact, three images of the same object point are required to ensure the accuracy of 3D reconstruction, so the overlap degree of the heading and adjacent track (side) is more than 66%.

The overlap rate is set to 66% during viewpoint filtering after determining the area that each camera can capture through visibility conditions. The viewpoint is retained if more than 66% of the area that can be captured by one camera is covered by another camera. If other cameras can see the area captured by the viewpoint, the camera is redundant and can be removed.

When $\theta_c^u \geq 0$, the UAV fuselage will appear in the field of view causing the fuselage to block the target. The range of $\gamma_c^u$ is $[-45^o \sim 45^o]$ due to the influence of PTZ's own structure. All viewpoints that do not fall within the aforementioned range of attitude angles must be removed during viewpoint filtering.

### 2.5 Camera incidence angle

The visual angle constraint cannot guarantee the quality of the captured image, and the image quality can be described by the image error. That the image error is related to the incident angle of the camera. When the incident angle is $60^o$, the pixel error will significantly increase. Therefore, the incident angle should satisfy the condition in (4) when screening the viewpoint:

$$\boldsymbol{n} \cdot \boldsymbol{v} \geq \|\boldsymbol{n}\| \|\boldsymbol{v}\| \cos 60^o \tag{4}$$

In this study, the included angle between the model mesh vertex and the camera axis is calculated for the model area that can be captured by each viewpoint when filtering viewpoints. When the proportion of incident angles that are greater than $60^o$ exceeds 20% of the total number of incident angles of the region's viewpoint to all mesh vertices, the viewpoint is deleted.

## 3 Discussion of results

### 3.1 Viewpoint planning

Planning the viewpoint position and attitude and generating the waypoint file are necessary after setting the camera position and attitude control parameters.

### 3.2 Candidate view area layout

After the UAV aerial photography is manually controlled, the approximate 3D model of the measured target is obtained during the placement of candidate viewpoints. The observation space is discretized by spherical surface and longitude and latitude division method. Since the object is above the earth's surface, only the hemisphere needs to be considered. The candidate viewpoint layout needs to determine the radius of the sphere, as well as the longitude and latitude. The radius of the ball is set through the number of pixels, focal length, and zoom distance to determine the shooting distance range.

### 3.3 Viewpoint supplement

The viewpoint is supplemented by the expansion method to preserve the integrity of the data. The expansion starting point is the plane centroid of the mesh patch in the missed area. The shooting distance is then expanded along the average vector direction of the model mesh patch, and the end point is the viewpoint position.

According to the constraints, candidate viewpoints are filtered to determine the sub-viewpoint set of viewpoint filtering. The ant colony algorithm is then used to plan the optimal flight path for the selected sub-view set. A waypoint file containing the UAV longitude, latitude, and altitude, as well as the heading, pitch and roll angles of the PTZ is generated for automatic aerial photography.

### 3.4 Experiment

According to the method proposed in this paper, experiments were carried out on the bronze statue of Pixiu with an outdoor height of more than 10m.

#### 3.4.1 Experimental platform

The diagram of the automatic aerial photography system is illustrated in Fig. 4. The system includes position and attitude control software and ground station to accurately control the position and attitude of the camera. The software out-in the waypoint file produced by the plan and uses the wireless data transmitter to send the waypoint to the flight order through the ground station. After receiving each waypoint command, the flight controller directs the UAV and the camera to carry out the corresponding actions. When the position and attitude of the specified viewpoint are reached, the software will send a signal to take a picture.

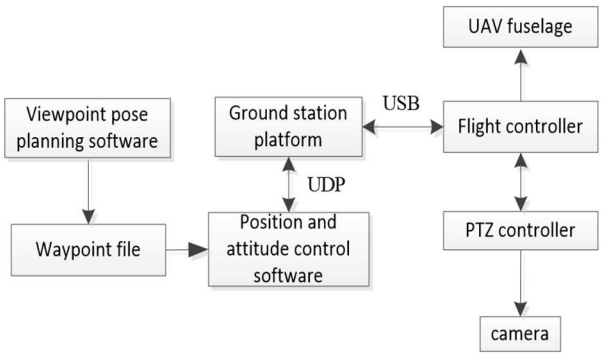


***Fig. 4*** *Diagram of automatic aerial photography system*

### 3.5 Experimental results and analysis

The viewpoint reconstruction results planned by the conventional approach and those planned by this method are compared to verify the proposed viewpoint planning. Fig. 5(a) illustrates image reconstruction results based on the proposed viewpoint planning method while the result in Fig. 5(b) is based on the conventional method. Compared with the inner part of the red rectangle, it can be seen that the reconstruction quality of the conventional method is poor.

(a) Result of viewpoint reconstruction planned with the proposed method

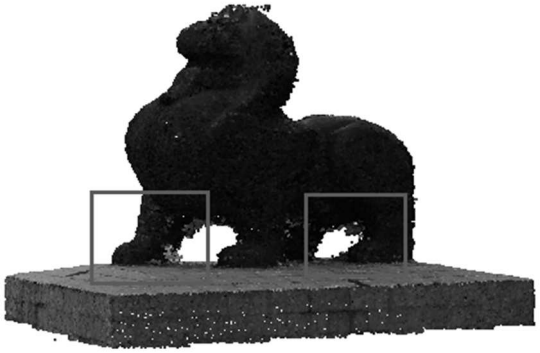

(b) Result of viewpoint reconstruction planned with the conventional method

***Fig. 5*** *Comparison of two reconstruction effects*

Point cloud data captured by the Leica P20 laser scanner with an accuracy of less than 1mm is considered as the reference model, and image reconstruction results using the our method are compared with those obtained by the conventional approach. Figure 6 displays the point cloud comparison deviation for the two methods, and Table 1 shows their data comparison results. The viewpoint placement approach suggested in this study exhibits better completeness and higher reconstruction accuracy.

(a) Reconstruction results based on the proposed method

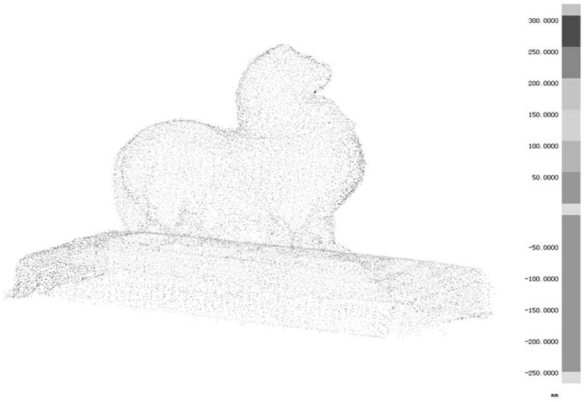

(b) Reconstruction results based on conventional methods

***Fig. 6*** *Point cloud comparison results*

***Tab. 2*** *Data comparison results for different methods*

| | **Methods in this paper** | **General method** |
|---|---|---|
| **Number of viewpoints** | 71 | 71 |
| **Rebuild the number of feature points** | 221473 | 173514 |
| **Average error of laser point cloud comparison** | 15.16 cm | 16.62 cm |
| **Standard error of laser point cloud comparison** | 13.08 cm | 13.78 cm |

## 4 Conclusion

This study focuses on the multi-view 3D reconstruction viewpoint layout. The appropriate camera position and attitude control parameters for multi-rotor UAV aerial photography with a single camera are determined, and the error model is established. A viewpoint planning and screening method based on known models is proposed considering visibility, camera incidence angle, overlap and coverage, as well as camera PTZ constraints. The high coverage of the proposed method is experimentally verified, and the final reconstruction

results are compared to the high-precision model obtained using a laser scanner, demonstrating that the image produced with the proposed approach has high reconstruction accuracy and is appropriate for image capture for large object three-dimensional reconstruction.

## Acknowledgement

***This research was supported by the School-level Research Projects of West Anhui University (WXZR202211), West Anhui University high-level Personnel Research Funding Project (WGKQ2022015), Anhui Provincial Quality Engineering Project (2021sysxzx031, 2022sx171), School level Quality Engineering Project of West Anhui University (wxxy2022085) , the Open Fund of Anhui Undergrowth Crop Intelligent Equipment Engineering Research Center (AUCIEERC-2022-05).***

## References

[1] LI, A.Y., YUAN, J.Y., PUN, C., BARENSE, M.D. (2023). The effect of memory load on object reconstruction: Insights from an online mouse-tracking task, *Attention, Perception, & Psychophysics*, Vol. 163, No.1, pp. 1-19.

[2] MA, K., WANG, X., HE, S., ZHANG, X., ZHANG, Y.X. (2023). Learning to image and track moving objects through scattering media via speckle difference, *Optics and Laser Technology*, Vol.159, pp. 108925.

[3] MATUŠ, M., BECHNÝ, V., JOCH, R., DRBÚL, M., HOLUBJÁK, J., CZÁN, A., NOVÁK, M. & ŠAJGALÍK, M. 2023. Geometric Accuracy of Components Manufactured by SLS Technology Regarding the Orientation of the Model during 3D Printing. *Manufacturing Technology*, 23, 233-40.

[4] ZHANG, Y., SHAO, H.C., PAN, T., MENGKE, T. (2023). Dynamic cone-beam CT reconstruction using spatial and temporal implicit neural representation learning (STINR), *Physics in Medicine & Biology*, Vol. 68, No. 4, pp. 045005.

[5] MAST, T.D., JOHNSTONE, D.A., DUMOULIN, C.L., LAMBA, M.A., PATCH, S.K. (2023). Reconstruction of thermoacoustic emission sources induced by proton irradiation using numerical time reversal, *Physics in Medicine & Biology*, Vol. 68, No. 2, pp. 025003.

[6] SEDLAK, J., JOSKA, Z., HRBACKOVA, L., JURICKOVA, E., HRUSECKA, D. & HORAK, O. 2022. Determination of Mechanical Properties of Plastic Components Made by 3D Printing. *Manufacturing Technology*, 22, 733-46.

[7] THIRUMALAI, A., RAMAN, P.G., JAYAVELU, T. (2023). Bridging the gap between maleate hydratase, citraconase and isopropylmalate isomerase: Insights into the single broad-specific enzyme, *Enzyme and Microbial Technology*, Vol. 162, pp. 110140.

[8] BAUER, D., WU, Q., MA, K.L. (2023). FoVolNet: Fast Volume Rendering using Foveated Deep Neural Networks, *IEEE Transactions on Visualization and Computer Graphics*, Vol. 29, No. 1, pp. 515-525.

[9] TONG, Y.D., CAI, Y.Z., NEVIN, A., MA, Q.L. (2023). Digital technology virtual restoration of the colours and textures of polychrome Bodhidharma statue from the Lingyan Temple, Shandong, China, *Heritage Science*, Vol. 11, No. 1, pp. 1-17.

[10] PERNICA, J., VODÁK, M., ŠAROCKÝ, R., ŠUSTR, M., DOSTÁL, P., ČERNÝ, M. & DOBROCKÝ, D. 2022. Mechanical Properties of Recycled Polymer Materials in Additive Manufacturing. *Manufacturing Technology*, 22, 200-3.

[11] MARTEL, C., ARNALSTEEN, C., LECOINTRE, L., LAPOINTE, M., ROY, C., FALLER, E., BOISRAMÉ, T., SOLER, L., AKLADIOS, C. (2023). Feasibility and clinical value of virtual reality for deep infiltrating pelvic endometriosis: A case report, *Journal of Gynecology Obstetrics and Human Reproduction*, Vol. 52, No. 1, 102500.

[12] LICHOVNÍK, J., MIZERA, O., SADÍLEK, M., ČEPOVÁ, L., ZELINKA, J. & ČEP, R. 2020. Influence of Tumbling Bodies on Surface Roughness and Geometric Deviations by Additive SLS technology. *Manufacturing Technology*, 20, 342-6.

[13] DIEZINGER, M.A., TAMADAZTE, B., LAURENT, G.J. (2022). 3d curvature-based tip load estimation for continuum robots, *IEEE Robotics and Automation Letters*, Vol. 7, No. 4, pp. 10526-10533.

[14] DU, G., DENG, Y., NG, W.W., LI, D. (2022). An Intelligent Interaction Framework for Teleoperation Based on Human-Machine Cooperation, *IEEE Transactions on Human-Machine Systems*, Vol. 52, No. 5, pp.963-972.

[15] JEON, M.H., KIM, J., RYU, J.H., KIM, A. (2022). Ambiguity-Aware Multi-Object Pose Optimization for Visually-Assisted Robot

Manipulation, *IEEE Robotics and Automation Letters*, Vol. 8, No. 1, pp.137-144.

[16] SCOTT, W.R., ROTH, G. (2023). View Planning for Automated Three-Dimensional Object Reconstruction and Inspection, *ACM Computing Surveys*, Vol. 35, No. 1, pp.61-96.

[17] FABIAN, M., HUŇADY, R. & KUPEC, F. 2022. Reverse Engineering and Rapid Prototyping in the Process of Developing Prototypes of Automotive Parts. *Manufacturing Technology*, 22, 669-78.

[18] PONIKELSKY, J., ZURAVSKY, I., CERNOHLAVEK, V., CAIS, J. & STERBA, J. 2021. Influence of Production Technology on Selected Polymer Properties. *Manufacturing Technology*, 21, 520-30.

[19] QIAN, R., LAI, X., LI, X.R. (2022). 3D Object Detection for Autonomous Driving: A Survey, *Pattern Recognition*, Vol. 130, pp. 108796.

[20] ZACCHINI, L., FRANCHI, M., RIDOLFI, A. (2022). Sensor-driven autonomous underwater inspections: A receding-horizon RRT-based view planning solution for AUVs, *Journal of Field Robotics,* Vol. 39, No. 5, pp.499-527.

[21] OLAGUE, G. (2007). Design and Simulation of Photogrammetric networks using Genetic algorithms, *ASPRS 2000 Annual Conference Proceeding*.

[22] MENDRICKY, R. & SOBOTKA, J. 2020. Accuracy Comparison of the Optical 3D Scanner and CT Scanner. *Manufacturing Technology*, 20, 791-801.

[23] DUNN, E., OLAGUE, G. (2004). Milti-objective Sensor Planning for Efficient and Accurate Object Recinstruction, *EvoWorkshops,* pp. 312-321.

[24] SCHMID, K., HIRSCHMULLER, H. (2012). View Planning for Multi-View Stereo 3D Reconstruction Using an Autonomous Multicopter, *Intel Robot Syst*, Vol. 65, pp.309-323.

[25] ZHEN, X. (2014). UAV aerial image-based three-dimensional reconstruction of outdoor scenes, *Zhejiang University of Technology*.

[26] GOSPODNETIĆ, P., MOSBACH, D., RAUHUT, M., HAGEN, H. (2022). Viewpoint placement for inspection planning, *Machine Vision and Applications*, Vol. 33, No. 2, pp. 1-21.